LBL-16486
Preprint c.2

Lawrence Berkeley Laboratory

UNIVERSITY OF CALIFORNIA

RECEIVED
LAWRENCE
BERKELEY LABORATORY
NOV 1 1983
LIBRARY AND
DOCUMENTS SECTION

Materials & Molecular Research Division

Submitted to the Journal of Chemical Physics

ANALYSIS OF THE OPTICAL SPECTRUM OF $Np(BD_4)_4$ DILUTED IN $Zr(BD_4)_4$ AND THE MAGNETIC PROPERTIES OF $Np(BH_4)_4$ AND $Np(BH_3CH_3)_4$

K. Rajnak, R.H. Banks, E. Gamp, and N. Edelstein

September 1983

TWO-WEEK LOAN COPY

This is a Library Circulating Copy which may be borrowed for two weeks. For a personal retention copy, call Tech. Info. Division, Ext. 6782.

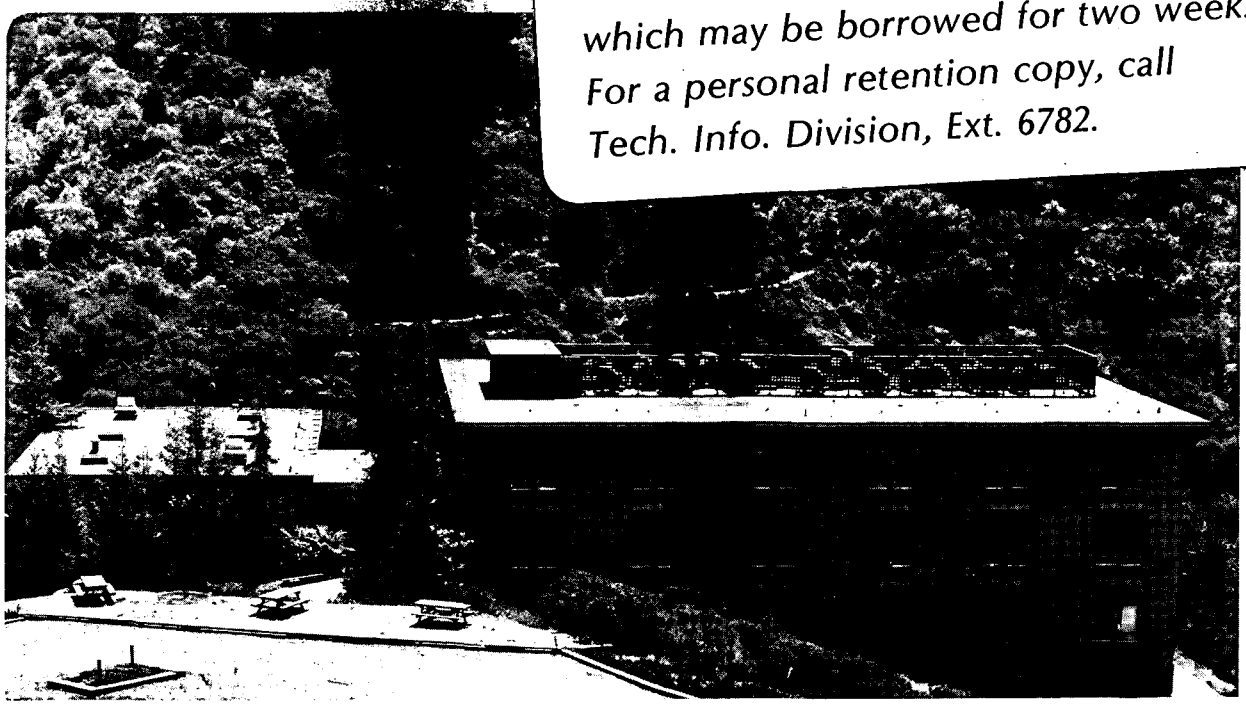

Prepared for the U.S. Department of Energy under Contract DE-AC03-76SF00098

LBL-16486 c.2

DISCLAIMER

This document was prepared as an account of work sponsored by the United States Government. While this document is believed to contain correct information, neither the United States Government nor any agency thereof, nor the Regents of the University of California, nor any of their employees, makes any warranty, express or implied, or assumes any legal responsibility for the accuracy, completeness, or usefulness of any information, apparatus, product, or process disclosed, or represents that its use would not infringe privately owned rights. Reference herein to any specific commercial product, process, or service by its trade name, trademark, manufacturer, or otherwise, does not necessarily constitute or imply its endorsement, recommendation, or favoring by the United States Government or any agency thereof, or the Regents of the University of California. The views and opinions of authors expressed herein do not necessarily state or reflect those of the United States Government or any agency thereof or the Regents of the University of California.

LBL-16486

Analysis of the Optical Spectrum of $Np(BD_4)_4$ Diluted in $Zr(BD_4)_4$ and the Magnetic Properties of $Np(BH_4)_4$ and $Np(BH_3CH_3)_4$[a]

K. Rajnak,* R. H. Banks**, E. Gamp, and N. Edelstein

Materials and Molecular Research Division
Lawrence Berkeley Laboratory
University of California
Berkeley, California 94720

Abstract

The optical spectrum of $Np(BD_4)_4/Zr(BD_4)_4$ is reported and analyzed. The parameter values obtained are consistent with those for $U(BD_4)_4/Hf(BD_4)_4$ (J. Chem. Phys., previous paper). A total of 46 levels were fit with $\sigma = 84\ cm^{-1}$. EPR data on $Np(BD_4)_4/Zr(BD_4)_4$ and $Np(BH_3CH_3)_4/Zr(BH_3CH_3)_4$ and the magnetic susceptibility of $Np(BH_3CH_3)_4$ are reported. They could be fit with the eigenvectors from the optical analysis only by the inclusion of orbital reduction factors k = 0.885 for $Np(BD_4)_4$ and 0.862 for $Np(BH_3CH_3)_4$. These values indicate greater covalency for the methylborohydride.

Introduction

At room temperature Np borohydride is a volatile, reactive liquid whose physical properties closely resemble those of Hf and Zr borohydrides rather than its neighbor in the periodic table,

$U(BH_4)_4$. It is monomeric in the solid state, and the local symmetry about the Np^{4+} ion is T_d.[1] This high symmetry plus the $5f^3$ electron configuration makes $Np(BH_4)_4$ an attractive candidate for magnetic and optical studies. In addition, our reanalysis[2] of Bernstein and Keiderling's spectra[3] of $U(BD_4)_4$ diluted in $Hf(BD_4)_4$ provides initial values for the crystal field parameters. In this paper we report detailed measurements and the analysis of the optical spectra of $Np(BD_4)_4$ diluted in $Zr(BD_4)_4$ as well as EPR measurements on this system. We also compare the average spin-Hamiltonian parameters of the closely related molecule $Np(BH_3CH_3)_4$ diluted in $Zr(BH_3CH_3)_4$ and report the measurement of the magnetic susceptibility of $Np(BH_3CH_3)_4$ from approximately 2 K - 300 K. In the following paper[4] a complete analysis of the unexpectedly anisotropic EPR spectra of $Np(BH_3CH_3)_4$ diluted in single crystals of $Zr(BH_3CH_3)_4$ is given.

Experimental

The preparation and purification of $Np(BH_4)_4$, $Zr(BH_4)_4$, their deuterated analogs, $Np(BH_3CH_3)_4$, and $Zr(BH_3CH_3)_4$ have been described previously.[1,5] Single crystals of pure $Np(BH_4)_4$ or $Np(BD_4)_4$ were grown by simply cooling the liquid (at room temperature) very slowly in a quartz cell placed in an optical dewar. When the sample temperature reached ~ 150 K, in approximately 8 hours, liquid helium was added which was subsequently

pumped below the lambda point. All spectra given in this paper were recorded on a Cary 17 spectrophotometer with the sample at ~ 2 K. Mixed crystals of $Np(BH_4)_4/Zr(BH_4)_4$ and $Np(BD_4)_4/Zr(BD_4)_4$ were grown from the vapor following the method of Bernstein and Keiderling.[3]

Spectra were also obtained with $Np(BH_4)_4$ or $Np(BD_4)_4$ isolated in a methylcyclohexane glass. These spectra were similar to those obtained in single crystals but had larger linewidths. In the photographic region, 300-900 nm, low temperature spectra of $Np(BD_4)_4/Zr(BD_4)_4$ were obtained on a 3/4 m Jarrell-Ash spectrograph with higher resolution than the Cary 17. No additional structure was observed.

For EPR measurements, approximately 50-100 mg of $Zr(BH_4)_4$ or $Zr(BD_4)_4$ were transferred to the bottom of a 3 mm ID quartz EPR tube. A small amount (~ 100 μg) of $Np(BH_4)_4$ or $Np(BD_4)_4$ was then condensed onto the Zr compound. Due to the size of the microwave cavities, the sample tubes could be no longer than 3 cm. The seal-off area on the quartz tube was kept at ~ 100 C during the transfer of the borohydrides by heating a nichrome wire wrapped around the area in order to prevent mirror formation on the tube (which appreciably lowered the cavity Q). The sample was held at 77 K during the seal off operation. The solid borohydride mixture was then melted to give a solution whose green color was barely perceptible. Following solidification of the liquid at one end of the tube, the other end was kept immersed in 1/4 in. of ice water for 15 hours. The resulting

vapor-grown single crystal was homogeneous and transparent.

The EPR measurements at X and Q bands were made at 4.2 K with Varian models E-101 (9 GHz) and E-110 (34.5 GHz) microwave bridges. The magnetic field was produced by a rotating electromagnet with a 2-5/8" gap (12" diameter polefaces, maximum field strength 10.8 kG) and measured with an Alpha Scientific NMR gaussmeter monitored by a frequency counter. K band spectra were obtained with a superheterodyne spectrometer at 1.7 K in the region 24-25 GHz. A George Associates rotating-coil gaussmeter was used to measure the magnetic field.

For the later experiments at 35 GHz on $Np(BH_3CH_3)_4$ samples, the magnet pole faces were changed so that a field of 16 kG could be obtained with a gap of 2". The preparation of single crystals of $Np(BH_3CH_3)_4$ diluted in $Zr(BH_3CH_3)_4$ and of $Np(BH_3CH_3)_4$ in a methylcyclohexane glass are described in the following paper.[4]

Magnetic susceptibility measurements were carried out as described previously.[2] One sample of $Np(BH_3CH_3)_4$ was measured with a nominal weight of 10 mg. Because of problems of obtaining an accurate weight on this small sample, the weight of the sample was adjusted so that the susceptibilities at low temperature agreed with the values calculated from the g value obtained by EPR measurements.

Results

Optical spectra of $Np(BD_4)_4/Zr(BD_4)_4$, $Np(BD_4)_4$,

$Np(BH_4)_4/Zr(BH_4)_4$, and $Np(BH_4)_4$ are shown in Figures 1 and 2. The $Np(BD_4)_4/Zr(BD_4)_4$ spectra have the narrowest linewidths and were chosen for a detailed analysis. Blanks were run on the Zr host crystals so as to be able to distinguish pure vibrational overtones from electronic and electronic plus vibrational transitions.

The EPR spectra for single crystals of $Np(BH_4)_4/Zr(BH_4)_4$ and $Np(BD_4)_4/Zr(BD_4)_4$ were isotropic and could be fit to the parameters of the spin-Hamiltonian

$$H = g\beta \underline{H} \cdot \underline{S}' + A\underline{I} \cdot \underline{S}' \qquad (1)$$

where the effective spin $S' = 1/2$, the nuclear spin $I = 5/2$ for the ^{237}Np nucleus, β is the Bohr magneton, g the g value, H the applied magnetic field, and A the hyperfine coupling constant. The values of g and A are given in Table I. The EPR spectrum of pure $Np(BD_4)_4$ consisted of one broad line (linewidth ~ 5000 gauss) centered at $g = 2.0 \pm .2$.

The EPR spectra of $Np(BH_3CH_3)_4$ diluted in $Zr(BH_3CH_3)_4$ were slightly anisotropic. However, for $Np(BH_3CH_3)_4$ dissolved in methylcyclohexane, an isotropic resonance was observed with the spin-Hamiltonian parameters shown in Table I. A detailed presentation and analysis of the data for the diluted crystal are given in the following paper. The average values of g and A for that system are given in Table I.

Table I shows the hyperfine coupling constant as 0.114 cm^{-1}. Because this constant is so large, we cannot make the usual assumption that the Zeeman term (the first term on the right hand side of Eq. (1)) is large compared to the hyperfine term. In order to fit the experimental spectra to the parameters of the spin Hamiltonian, the exact energies obtained from the Breit-Rabi equation,[6] were used. In fact at X-band frequencies, ~ 9.4 GHz, the zero field splitting, 3A, was greater than the microwave energy, so that only four transitions were observed. The spectra at X-band and at 24 GHz are shown in Figure 3. The energy level diagram showing the various transitions is given in Figure 4.

For a $5f^3$ ion, a J = 9/2 multiplet will lie lowest. In T_d symmetry this multiplet splits into one Γ_6 and two Γ_8 states. The Γ_8 states should show anisotropic behavior in a magnetic field so we assign the observed EPR resonances to the isotropic Γ_6 state. This fixes the symmetry of the ground crystal field state for the following optical analysis.

The reciprocal of the magnetic susceptibility of pure $Np(BH_3CH_3)_4$ vs. temperature is shown in Figure 5. Considering only the $^4I_{9/2}$ ground term (a bad approximation), curve A was obtained with crystal field parameters, $B_0^4 = -1460.7$ cm^{-1}, $B_0^6 = -3274.4$ cm^{-1}, and the orbital reduction factor k = 0.82.

Optical Analysis

The absorption lines of $Np(BD_4)_4/Zr(BD_4)_4$ are given in

Table II. The vibrational energies of $Np(BD_4)_4$ have been determined from the IR and Raman spectra.[7,8] Table III shows the corresponding energies of vibrations associated with the various origins as identified in this analysis. The assignments for some of the lower levels are discussed in detail below. The designation of the vibrations is the same as that in the previous paper[2] which retained, insofar as possible, the notation of Bernstein and Keiderling.[3] Some vibrations appear here which were not clearly identified in the $U(BD_4)_4$ analysis. The data were analyzed with the same Hamiltonian[9,10] used for $U(BD_4)_4/Hf(BD_4)_4$, but with the addition of the 3-body configuration interaction parameters[11] T^k which do not arise for f^2 configurations.

From the Γ_6 ground state found from the EPR measurements, transitions are allowed to both Γ_7 and Γ_8 states; all vibrations can couple with Γ_8 states and all but T_2 vibrations can couple with Γ_7's. Since there is only one vibration with T_2 symmetry, this is not of much help in making assignments. Consequently, they were based on the following criteria:

1) the ability to assign a consistent set of vibrational energies associated with given origin;

2) agreement between calculated and experimental energies;

3) association of origins with sharp lines unless vibronics from another origin have nearly the same energy;

4) assignment of the strongest lines as origins unless that conflicted strongly with 1) and 2).

These criteria provide neither a clear distinction between origins and vibrations nor a unique association between origins and particular Γ_7 or Γ_8 states.

Somewhat more useful was the additional requirement that

5) the resultant parameter values bear expected relationships to those of $U(BD_4)_4$.

We expected the crystal field parameters of $U(BD_4)_4$ and $Np(BD_4)_4$ to be nearly the same. Two different approaches were taken to establishing an expected range of the free-ion parameters. Pseudo-relativistic Hartree-Fock (HFR) functions were calculated for U^{4+} and Np^{4+} with the code of Cowan and Griffin.[12] (See Table IV). It was assumed that the differences between the HFR values of F^2, F^4, F^6 and ζ and the values for the borodeuterides would be the same for both U^{4+} and Np^{4+}. Since the U^{4+} free ion spectra have been analyzed,[13] the same procedure can be used to estimate the free-ion parameters for Np^{4+}. The second approach to the borodeuteride parameters was the assumption that the differences between the $U(BD_4)_4$ and $Np(BD_4)_4$ parameter values would be the same as those found for U^{3+} and Np^{3+} substituted in $LaCl_3$[14] (Table V). These considerations led us to expect parameters for neptunium borodeuteride in the following ranges:

$F^2 = 44400 - 46500\ cm^{-1}$, $F^4 = 42069 - 43400\ cm^{-1}$
$F^6 = 24080 - 24600\ cm^{-1}$, $\zeta = 2065 - 2090\ cm^{-1}$ and to
predict $F^2 = 54463$ and $\zeta = 2253\ cm^{-1}$ for the Np^{4+} free ion.

The preliminary results referred to previously[15] relied heavily on the assignment of the strongest lines as origins. About 30 levels could be fit with $\sigma \sim 80\ cm^{-1}$ but criterion 5 was not satisfied. B_0^4 was $\sim -5000\ cm^{-1}$ vs. -2448 for $U(BD_4)_4/Hf(BD_4)_4$. F^2 was $\sim 42000\ cm^{-1}$, the same as for $U(BD_4)_4$ and much lower than expected.

Therefore we began again, changing some of the infrared assignments, fixing parameters where necessary to keep them in the right range, gradually adding levels until most of the parameters could be fit. Those levels which deviated most from the calculations were continually reexamined to see if another choice of origin could fit the calculation better and still allow reasonable assignment of the vibrations. With the close spacing of the levels and the large number of different vibrational frequencies, this was often possible. It did require, however, that in some cases the strongest line in a group be assigned as a vibronic transition rather than as an origin. The same was true for some $U(BD_4)_4$ transitions.

The final assignments given in Table II are certainly not unique, and they are not independent of the calculations. Some of the lower levels are discussed in detail below.

1) origin a, $5605\ cm^{-1}$

The differences in intensity of the vibronics involving various groups of vibrations are clearly seen in Fig. 1. The origin is followed by a strong group of lines involving a single phonon in the

100-200 cm^{-1} energy range (β, δ, and ϵ of Table III). These vibronics are nearly as sharp as the origin. The weak and broader transitions involving multiples of these phonons are followed by another strong, sharp group involving single phonons in the 400-500 cm^{-1} energy range (ζ, n', η, θ). Weak transitions involving one phonon from each of the two groups are followed by another set of vibronics with single phonons of 800-950 cm^{-1} (γ, χ, Ξ, λ, λ'). The one-phonon vibronics with energies ~ 1500 cm^{-1} (ξ, ξ', ξ'') seen at ~ 1400 nm in Fig. 2 are almost as strong as the first group. One possible interpretation of the weak transitions at ~ 1180 nm is as vibronics involving two of these phonons.

The very weak broad peak immediately following the origin (designated xx in Tables II and III) is of too low a frequency to correspond to a vibration of the $Np(BD_4)_4$ molecule. It must be attributed to a lattice mode. A similar weak transition occurred in the $U(BD_4)_4/Hf(BD_4)_4$ spectrum although the energy was 114 cm^{-1}.

There is another vibrational energy, 138 cm^{-1}, designated xxx in Table III, which cannot be associated with any of the normal modes of the $Np(BD_4)_4$ molecule. This one is associated with a strong, sharp vibronic, however. It also appears coupled in multiphonon vibronics of origin a but is not associated with any other origins.

In the IR spectrum Banks and Edelstein[7] observed two vibrations at 437 and 457 cm^{-1} which were assigned to the same vibrational mode, but the 457 cm^{-1} vibration was associated with ^{10}B rather

than ^{11}B. The ^{10}B vibration was weaker as expected from the relative abundances of ^{11}B and ^{10}B. When associated with origin a, these energies are 430 and 452 cm^{-1}, but the higher energy one is much more intense. These vibrations are designated η' and η in Tables II and III. No attempt has been made to confirm the ^{10}B assignment. The two vibrations appear together only with origin a and the stronger one, η, is more frequently observed.

2) Origin b, 7083 cm^{-1}

As seen in Fig 2, this strong sharp line, which certainly looks like an origin, nearly disappears in the pure $Np(BD_4)_4$ spectrum. If we assign this line as a forbidden transition that has become allowed due to a slight lowering of the T_d symmetry in the $Zr(BD_4)_4$ crystal, we have two problems: the isotropy of the ground state g value and the lack of evidence for two transitions. Many of our calculations placed Γ_6 and Γ_8 levels ~ 50 cm^{-1} apart in this region with the Γ_6 lower. The Γ_8 assigned to this origin fit very poorly. If part of the intensity is due to a vibronic of the forbidden Γ_6 level, the separation between the Γ_6 and Γ_8 would be that of the β or δ-vibration, ~ 120 or ~ 160 cm^{-1}, instead of 50 cm^{-1}. Both levels would then fit very poorly in the calculations. The final calculation puts the Γ_6 and Γ_8 levels only 0.3 cm^{-1} apart. Consequently, we cannot rule out the possibility that the two levels are very nearly degenerate and that the enhanced intensity in the dilute crystal is somehow related to

this fact.

As seen in Tables II and III most of the vibrations associated with origin a are associated with b also. A few of these have 10-15 cm^{-1} differences in energy.

3) Origin c, 7594 cm^{-1}

We first assigned origin c as the very strong transition at 7690 cm^{-1}. It was possible to fit a group of 30 or 40 levels with this as one of the assignments, but the deviation of this level was always > 200 cm^{-1} when σ was ~ 100 cm^{-1}. When this level and the previous one were weighted 50 times as strongly as the others, it was again possible to obtain σ ~ 100 cm^{-1}, now with these levels fitting very well, but with F^4 ~ 40000 and B_0^4 ~ -4700 cm^{-1}. These are both well outside the expected ranges.

A further reason for rejecting this strong line as an origin is the lack of strong vibronics associated with it. In general, the intensity of the electronic transition is reflected in at least the first vibronics. It is possible to assign five reasonable vibrational energies with this as an origin, but three of these are observed only in combinations.

If the transition at 7690 cm^{-1} is to be assigned as a vibronic, the origin must be one of the sharp transitions at 7642 or 7694 cm^{-1}. The lower one is in better agreement with the calculations, but a larger number of vibronics can be assigned with the higher one as the origin. Furthermore, this transition has a less likely

explanation as a vibronic of b. Consequently, 7694 has been chosen as an origin. With this choice, all of the transitions up to 9000 cm^{-1} can be assigned as vibronics associated with origins a, b, and c.

The strong transition at 7690 cm^{-1} must be interpreted as a vibronic associated with the β vibration (96 cm^{-1}) and/or the η vibration associated with the Γ_6 level calculated at 7193 cm^{-1}. Some of the intensity of this line could also come from vibronics of origin b. The lack of an ε vibronic associated with c is consistent with its assignment as a Γ_7 level.

4) Origins d and e, 9281 and 9571 cm^{-1}

The next group begins with a weak but sharp line at 9281 cm^{-1} which cannot be easily associated with a vibronic of origin c. It is the only line which is appreciably stronger in the pure than in the dilute crystal. The large number of one- and two-phonon vibronics which can be associated with it make this assignment (origin d) quite certain. The β vibration is assigned to the sharp line at 9403 which is four times as intense. A similar intensity ratio for origin c and its β vibronic would account for more than half of the intensity of the peak at 7690 cm^{-1}.

The assignment of origin e is less clear-cut. The strong line at 9449 cm^{-1} could be all or partly due to the δ vibronic of d. If it is chosen as origin e, then the β vibronic is the relatively strong line at 9571 cm^{-1}, but the δ is a very weak broad line better associated with multiple phonons. If 9571 cm^{-1} is chosen as origin,

then the β and δ vibronics are both sharp and intense. This is more consistent with the assignment of those vibronics associated with other origins. Thus 9571 cm^{-1} was chosen as the origin.

The strong sharp line at 10335 cm^{-1} must then be explained as a sum of vibronics associated with origins d and e. The much lower intensity of this line in pure $Np(BD_4)_4$ is more consistent with such an interpretation. There is no way in which this line can be fit as an origin with parameters within the expected range.

5) Origin f, 10709 cm^{-1}

The most obvious choice of an origin in this region is the rather broad line at 10576 cm^{-1}, but it fits the calculations very poorly. That leaves either the line at 10709 or the one at 10796 cm^{-1}. Despite its width, we have chosen the former because of the impossibility of associating vibronics with the higher one. The width of the 10709 cm^{-1} line can be explained by near coincidence with vibronics of d and e. The line at 10796 cm^{-1} is well explained as the ξ vibronic of d.

6) Higher origins

The assignments of the strong origins g–n was fairly straightforward, but beyond 14000 cm^{-1} the lines are less sharp and generally weak. Fewer and fewer vibronics are seen. This is associated with both the decreasing intensity and decreasing resolution. As we have assigned the levels, the more intense origins

generally do exhibit vibronics. But without the vibronics, the choice of origins is more ambiguous. Some of the sharp lines which look most like origins fit the calculations very poorly. This could be due either to erroneous identification as origins or to the breakdown of the crystal field model. A vibronic intensity analysis is needed to verify the assignments.

The final assignments are shown in Tables II and III. The parameters are given in Table V and the observed and calculated levels are compared in Table VI. The rms deviation σ is 84 cm^{-1} for 46 levels.

Discussion

The observed levels cover less than half of the entire spread of the $5f^3$ configuration in this crystal and, without the higher levels, F^4 and F^6 cannot be uniquely determined. Likewise, the T^k, P^k parameters and β must be regarded as only very approximately determined. Attempts to fit β or T^2 reduced σ by only ~ 1 cm^{-1}.

In spite of this uncertainty in the free ion parameter values, it is clear that significant improvement in the fit cannot come from changes in these values; modification of the crystal field Hamiltonian appears to be necessary.

Already in $U^{4+}/ThBr_4$[16] where the crystal field is ~ 2.5 times smaller than in the borodeuterides, there was evidence for the breakdown of the crystal field model. The fit was worse for

$U(BD_4)_4/Hf(BD_4)_4$, but the large differences between experimental and calculated levels were still confined to relatively few states. For $Np(BD_4)_4$, however, levels which fit well are the exceptions. The higher density of states for f^3 increases J-mixing and seems to magnify the problems.

The borodeuteride data is probably not the place to test a new crystal field model, however. The large number of vibronic transitions gives rise to too many ambiguities in the identification of electronic origins. A new model should be tested in a system in which the levels are identified with more certainty. Of the currently available data, that for $U^{4+}/ThBr_4$ would probably be the best test case.

The parameter values shown in Table V are good enough to allow some tentative conclusions regarding relative covalency in $U(BD_4)_4/Hf(BD_4)_4$ and $Np(BD_4)_4/Zr(BD_4)_4$ and in the tetravalent vs. trivalent actinides. With few exceptions, for d^N series fluorides in the same oxidation state covalency (as measured by decreases in the nephalauxetic ratio $\beta = B/B_{free\ ion}$) increases with increasing atomic number.[17] If the Racah parameters B and C are transformed to F^k's, the effect is the same, i.e. $\phi_2 = F^2/F^2_{free\ ion}$ decreases with increasing Z. Although C is often poorly determined, the same effect is reflected in increasing ratios C/B or $r_{42} = F^4/F^2$ along a d^N series. This measure has the advantage of not requiring knowledge of the free ion parameters. The results of Crosswhite et al.[14] show that, contrary to the d^N

series, r_{42} decreases with Z for the trivalent actinides; r_{42} is 0.84 for U^{3+}:$LaCl_3$ and 0.81 for Pu^{3+}:$LaCl_3$. This is the result of the actinide contraction and increased screening of the 5f electron as Z increases. For the borodeuterides we find that r_{42} decreases from 0.97 to 0.93 in going from uranium to neptunium. Using the predicted value of 2253 cm^{-1} for $\zeta_{free\ ion}$ of the Np^{4+}, we find that $k = \zeta/\zeta_{free\ ion}$ increases from 0.91 to 0.93. The predicted value of F^2 for the Np^{4+} free ion leads to ϕ_2 of .86 for Np^{4+} vs. .81 for U^{4+}. These numbers are all consistent with increasing covalency with increasing oxidation number (as in the nd^N series) and decreasing covalency with increasing Z for both the trivalent and tetravalent actinides. A crude model[18] where the actinide wave function is written as

$$\Psi = a\psi_{metal} + b\psi_{ligand}$$

predicts that, to a first approximation, the free-ion value of ζ is multiplied by a^2 and F^2 by a^4, i.e. $\phi_2 \simeq k^2$. Our results are consistent with such a model.

Since the matrix elements of T^2 are not linearly independent of those of the F^k's, there is, in principle, a problem in comparing, as we have done above, calculations for f^3 (where T^2 is included) to those for f^2 where there is no T^2. Judd et al.[19,20] have suggested an alternate parameterization scheme, using orthogonalized operators, in which this problem does not arise. Table VII shows the Slater parameters and the new α', β', and γ' calculated from the results in Table V via the formulas of Ref. 20. Since F^2 is smaller

and F^4 relatively unchanged, the ratios r_{42} are all slightly larger. There is a larger difference in the ϕ_2 values for U^{4+} and Np^{4+} when the orthogonalized parameters are used. There are no differences in the trends, however; thus the conclusions drawn from the usual parameterization scheme remain unchanged.

From the wavefunctions and energies obtained from the optical analysis of $Np(BD_4)_4/Zr(BD_4)_4$, the reciprocal of the magnetic susceptibility vs. temperature and the ground Γ_6 state g value were calculated. Curve B in Fig. 5 shows the calculated reciprocal susceptibility. Table VIII gives the g values obtained for various values of the orbital reduction constant, k. With k = 0.862 the reciprocal magnetic susceptibility shown as curve C in Fig. 5 was obtained.

Without the introduction of the orbital reduction factor, the calculated g value for the ground state was too large. A lower value of k is needed to fit the methylborohydride g value, suggesting greater covalency in this molecule. Comparison of the k values for $U(BH_3CH_3)_4$ and $Np(BH_3CH_3)_4$ (Table VII) indicates somewhat less covalency for the neptunium compound. This is consistent with the optical results discussed above. In both the uranium and neptunium compounds the k from the optical analysis, which is an average over many levels, is larger than the k from the magnetic analysis which is sensitive only to the lower energy states.

It is noteworthy that the magnetic susceptibility of $Np(BH_3CH_3)_4$ could be fit within experimental error using the

energies and wavefunctions of the $Np(BD_4)_4/Zr(BD_4)_4$ analysis and adjusting only the orbital reduction factor. By contrast, the energy difference between the ground state and the first excited state also had to be adjusted in order to fit the $U(BH_3CH_3)_4$ data. However, for the Np compound there is a first order magnetic effect for the ground state which dominates the susceptibility while for the U compound the second order term is dominant because of the non-magnetic nature of the ground state.

Although a good fit to the magnetic data could be obtained by considering only the isolated $^4I_{9/2}$ term, the crystal field parameters and energy levels obtained are very different from those derived from the analysis of the optical data. One could be seriously misled by use of this oversimplified model if the criteria were only the agreement between the calculated susceptibility and g value and the experimental magnetic data.

Conclusions

The energy levels of $Np(BD_4)_4/Zr(BD_4)_4$ have been analyzed with vibronic assignments and energy parameters which are consistent with those found for $U(BD_4)_4/Hf(BD_4)_4$. The least squares fit is worse, however; σ is 84 cm^{-1} for the neptunium crystal whereas it was 71 or 53 cm^{-1} for uranium borodeuteride, depending on the choice of assignments. The free-ion parameters are not very well determined, but it is clear that a significant improvement in the fit will be possible only by modification of the crystal field Hamiltonian or

changes in many of the assignments.

If ϕ_2, r_{42} and k are used as measures of covalency, the parameter values indicate that covalency decreases with Z for the actinides and that the tetravalent actinides are more covalent than the trivalent actinides.

The magnetic data for $Np(BD_4)_4$ and $Np(BH_3CH_3)_4$ can be fit with the wavefunctions and energies obtained from the optical data only by the use of an orbital reduction factor. The values obtained for this parameter indicate that the methylborohydride compound is the more covalent.

Acknowledgments

We wish to thank John Conway for helpful discussions.

References

[a]This work was supported by the Director, Office of Energy Research, Office of Basic Energy Sciences, Chemical Sciences Division of the U.S. Department of Energy under Contract No. DE-AC03-76SF00098.

*Permanent address: Department of Physics, Kalamazoo College, Kalamazoo, Michigan 49007.

**Nalco Chemical Co., 1801 Diehl Road, Naperville, Il. 60540.

1. R. H. Banks, N. M. Edelstein, B. Spencer, D. H. Templeton, and A. Zalkin, J. Am. Chem. Soc. 102, 620 (1980).
2. K. Rajnak, E. Gamp, R. Shinomoto, and N. Edelstein, J. Chem. Phys. (preceding paper).
3. E. R. Bernstein and T. A. Keiderling, J. Chem. Phys. 59, 2105 (1973).
4. E. Gamp and N. Edelstein, J. Chem. Phys., following paper.
5. R. Shinomoto, E. Gamp, N. M. Edelstein, D. H. Templeton, and A. Zalkin, Inorg. Chem. (1983), in press.
6. G. Breit and I. Rabi, Phys. Rev. 38, 2002 (1931); see also: N. F. Ramsey, Molecular Beams, Oxford University Press, London, 1956, p. 86.
7. R. H. Banks and N. Edelstein, J. Chem. Phys. 73, 3589 (1980).

8. R. H. Banks and N. M. Edelstein in Lanthanide and Actinide Chemistry and Spectroscopy, N. Edelstein, Ed., ACS Symposium Series 131, Washington, D.C., 1980, p. 331.

9. W. T. Carnall, H. Crosswhite, H. M. Crosswhite, J. P. Hessler, N. M. Edelstein, J. G. Conway, G. V. Shalimoff, and R. Sarup, J. Chem. Phys. 72, 5089 (1980).

10. B. G. Wybourne, Spectroscopic Properties of Rare Earths, John Wiley and Sons, Inc., New York, 1965. Our definition for the crystal field parameters follows Wybourne's convention.

11. B. R. Judd, Phys. Rev. 141, 4 (1966).

12. R. D. Cowan and D. C. Griffin, J. Opt. Soc. Am. 66, 1010 (1976).

13. C. H. H. Van Deurzen, K. Rajnak, and J. G. Conway, J. Opt. Soc. Amer., 1983, submitted.

14. H. M. Crosswhite, H. Crosswhite, W. T. Carnall, and A. P. Paszek, J. Chem. Phys. 72, 5103 (1980).

15. K. Rajnak, E. Gamp, R. Banks, R. Shinomoto, and N. Edelstein, Inorg. Chim. Acta, to be published.

16. P. Delamoye, K. Rajnak, M. Genet, and N. Edelstein, Phys. Rev. B, in press.

17. D. C. Allen and K. D. Warren, Structure and Bonding 9, 49 (1971), 19, 105 (1974).

18. M. Gerloch and R. C. Slade, Ligand-Field Parameters, Cambridge Univ. Press, New York, 1973, p. 213.

19. B. R. Judd, Jorgen E. Hansen, and A. J. J. Raassen, J. Phys. B 15, 1457 (1982).

20. B. R. Judd and H. Crosswhite, J. Opt. Soc. B, to be published.

Table I. Spin Hamiltonian Parameters for ^{237}Np Borohydrides

Host	$Zr(BH_3CH_3)_4$ [a]	$CH_3C_6H_{11}$ [b]	$Zr(BH_4)_4$ [c]	$Zr(BD_4)_4$ [d]
g	1.7997(4) [e]	1.8126(4)	1.894(2)	1.891(2)
A (cm^{-1})	0.1122(2)	0.1124(1)	0.1140(10)	0.1140(10)

[a] $^{237}Np(BH_3CH_3)_4/Zr(BH_3CH_3)_4$.
[b] frozen solution (glass).
[c] $^{237}Np(BH_4)_4/Zr(BH_4)_4$.
[d] $^{237}Np(BD_4)_4/Zr(BD_4)_4$.
[e] averaged ("isotropic") values.

Table II. Absorption spectrum of $Np(BD_4)_4/Zr(BD_4)_4$ at 2 K: summary of electronic and vibrational assignments

λ(nm)	Estimated Uncertainty (± nm)	Relative Intensity	Vacuum Corrected Energy (cm^{-1})	Assignment to Origins + Δν (cm^{-1})	Vibrational Identification
1783.8	0.15	42	5605	origin a	
1770.0	0.5	4	5648	a + 43	xx
1746.1	0.2	24	5726	a + 121	a + β
1740.9	0.2	17	5743	a + 138	xxx
1735.4	0.2	17	5761	a + 156	a + δ
1730.6	0.2	29	5777	a + 172	a + ε
1710.4	0.3	3	5845	a + 240	a + 2β
1705.3	0.3	2	5863	a + 258	a + β + xxx
1700.6	1.0	1.5	5879	a + 274	a + β + δ
1695.7	0.3	5	5896	a + 291	a + β + ε
1690.2	0.5	1.5	5915	a + 310	a + 2δ
1680.0	1.0	0.5	5951	a + 346	a + 2ε
1670.0	0.6	1	5986	a + 381	a + 2β + xxx
1662.4	1.0	0.4	6014	a + 409	a + ζ
1656.5	0.3	4	6035	a + 430	a + η'
1650.6	0.2	22	6057	a + 452	a + η
1644.6	0.2	10	6079	a + 474	a + θ
1624.6	0.5	1	6154	a + 549	a + η' + β
1618.3	0.4	3	6177	a + 572	a + η + β
1613.5	0.9	2	6196	a + 591	a + xxx + η
1562.6	0.3	4	6398	a + 793	a + χ
1560.1	0.2	9	6408	a + 803	a + κ
1550.9	0.3	2	6446	a + 841	a + ζ + η'
1545.0	0.2	7	6471	a + 866	a + Ξ

Table II. Continued

λ(nm)	Estimated Uncertainty (± nm)	Relative Intensity	Vacuum Corrected Energy (cm^{-1})	Assignment to Origins + Δν (cm^{-1})	Vibrational Identification
1533.5	1.5	3	6519	a + 914	a + λ
1530.0	1.0	4	6534	a + 929	a + λ'
1516.6	0.6	1	6592	a + 987	a + 2η' + β
1411.4	0.1	98	7083	origin b	
1403.9	0.2	19	7121	a + 1516	a + ξ
				b + 38	b + xx
1400.9	0.3	21	7136	a + 1531	a + ξ'
1398.8	0.6	19	7147	a + 1542	a + ξ"
1388.2	0.4	15	7202	b + 119	b + β
1378.8	0.3	35	7251	b + 168	b + δ
				a + 1646	a + ξ' + β
1375.5	0.25	37	7268	b + 185	b + ε
				a + 1663	a + ξ" + β
1367.5	1.5	15	7311	a + 1706	a + ξ' + ε
1354.5	1.0	12	7381	b + 298	b + β + ε
				a + 1776	a + ξ" + 2β
1348.2	1.0	9	7415	b + 368	b + 2ε
1333.3	0.5	8	7498	b + 415	b + ζ
1325.6	0.2	32	7542	b + 459	b + η
1316.5	0.3	28	7594	origin c	
				b + 511	b + 3δ
1313.2	0.3	25	7613	b + 530	b + 2ε + δ
					b + β + ζ
1300.0	2.0	~ 230	7690	c + 96	c + β
				b + 607	b + δ + η
					b + ζ + ε
1273.5	0.6	20	7850	c + 256	c + β + δ
1267.4	0.5	16	7887	c + 294	c + 3β

Table II Continued

λ(nm)	Estimated Uncertainty (± nm)	Relative Intensity	Vacuum Corrected Energy (cm^{-1})	Assignment to Origins + Δν (cm^{-1})	Vibrational Identification
1263.9	1.0	15	7910	c + 316	c + 2δ
				b + 827	b + κ
1260.9	0.5	14	7929	b + 846	b + Ξ
1248.8	0.3	13	8006	b + 923	b + λ'
				c + 412	c + ζ
1241.8	0.5	12	8051	c + 457	c + η
1225.8	1.0	25	8156	c + 562	c + η + β
				b + 1073	b + Ξ + 2β
1178.0	0.6	7	8487	c + 893	c + λ
1173.0	0.9	5	8523	c + 929	c + λ'
1162.4	0.5	6	8601	b + 1518	b + ξ
				c + 1037	c + λ' + β
1158.3	1.2	7	8631	b + 1548	b + ξ"
				a + 3026	a + 2ξ
1152.4	1.2	5	8675	c + 1081	c + λ' + δ
				a + 3070	a + 2ξ'
1128.2	1.7	3	8861	b + 1778	b + Ξ + λ'
				c + 1267	c + λ' + 2δ
1077.2	0.4	5	9281	origin d	
1071.2	1.5	3	9333	d + 52	d + xx
1063.2	0.2	19	9403	d + 122	d + β
1058.0	0.15	45	9449	d + 168	d + δ
1050.2	0.2	4	9519	d + 238	d + 2β
1044.5	0.2	15	9571	origin e	
				d + 290	d + β + δ
1040.0	0.7	3	9613	d + 332	d + 2δ
				e + 48	e + xx
1030.0	1.3	12	9706	d + 425	d + η'

Table II Continued

λ(nm)	Estimated Uncertainty (± nm)	Relative Intensity	Vacuum Corrected Energy (cm^{-1})	Assignment to Origins + Δν (cm^{-1})	Vibrational Identification
1026.8	0.2	20	9736	d + 455	d + η
				e + 165	e + δ
1014.0	0.5	3	9859	d + 578	d + β + η
				e + 288	e + β + δ
1001.3	0.3	6	9984	d + 703	d + η + 2β
				e + 413	e + ζ
997.0	0.2	13	10027	e + 456	e + η
991.8	0.2	12	10080	d + 799	d + χ
985.2	0.2	9	10147	d + 866	d + Ξ
980.0	0.5	10	10201	d + 920	d + λ
967.3	0.15	80	10335	d + 1054	d + λ + β
				e + 764	e + χ
953.5	0.2	19	10485	e + 914	e + λ(2η)
945.3	0.3	27	10576	d + 1295	d + λ + 3β
				e + 1005	e + χ + 2β
933.5	1.2	9	10709	origin f	
				d + 1428	d + δ + η + χ
				e + 1138	e + λ + 2β
926.0	0.2	8	10796	d + 1515	d + ξ
918.8	1.5	4	10881	f + 172	f + ε
898.9	0.3	7	11122	f + 413	f + ζ
894.7	0.9	4	11174	f + 465	f + θ
866.7	1.0	~ 180	11535	origin g	
				f + 826	f + κ(2ζ)
855.7	0.8	50	11683	g + 148	g + δ
845.7	1.3	7	11821	g + 286	g + 2δ
834.6	0.2	62	11978	g + 443	g + η

Table II Continued

λ(nm)	Estimated Uncertainty (± nm)	Relative Intensity	Vacuum Corrected Energy (cm^{-1})	Assignment to Origins + Δν (cm^{-1})	Vibrational Identification
821.5	0.1	165	12170	origin h	
807.0	5.0	> 400	12388	h + 218	g + 2β
				g + 853	g + Ξ
792.0	~ 2.5	~ 55	12623	origin i	
				h + 453	h + η
780.0	~ 4.0	~ 30	12817	i + 194	i + ε
				h + 647	h + η + ε
771.2	1.0	93	12963	origin j	
				h + 793	h + χ
768.7	0.2	101	13005	j + 42	j + xx
				h + 835	h + κ
				i + 383	i + 2ε
764.1	1.0	78	13084	h + 914	h + λ
				j + 121	j + β
				i + 461	i + η
745.2	1.0	22	13416	origin k	
				j + 453	j + η
738.9	0.2	37	13530	k + 114	k + β
				j + 567	j + β + η
725.6	0.2	100	13778	origin ℓ	
				k + 248	k + 2β
718.8	0.7	66	13908	ℓ + 130	ℓ + β
713.8	0.2	66	14006	origin m	
706.1	0.5	43	14158	m + 152	m + δ
695.7	0.4	38	14370	origin n	
692.4	1.4	32	14439	origin o	
685.5	1.2	26	14584	o + 145	o + δ
				ℓ + 806	ℓ + κ

Table II Continued

λ(nm)	Estimated Uncertainty (± nm)	Relative Intensity	Vacuum Corrected Energy (cm^{-1})	Assignment to Origins + Δν (cm^{-1})	Vibrational Identification
675.9	0.6	32	14791	origin p	
670.6	0.3	23	14908	p + 117	p + β
664.7	1.5	15	15040	p + 249	p + 2β
				o + 601	o + δ + η
654.7	0.5	17	15270	origin q	
				ℓ + 1493	ℓ + ξ
				p + 479	p + θ
				o + 831	o + κ
650.5	2.0	14	15369	q + 99	q + β
				o + 930	o + λ'
642.4	0.4	9	15562	q + 292	q + 3β
				p + 771	p + χ
635.9	1.2	8	15721	q + 451	q + η
				p + 930	p + λ'
629.2	0.7	6	15889	origin r	
				p + 1098	p + λ' + δ
				q + 619	q + η + δ
616.2	0.3	7	16224	origin s	
				q + 954	q + λ'
613.2	0.3	11	16303	p + 1512	p + ξ
				r + 414	r + ζ
602.2	0.2	46	16601	origin t	
584.1	1.0	11	17116	origin u	
583.0	0.8	11	17148	s + 924	s + λ'
570.0	2.0	4	17539	u + 423	u + η'
				t + 938	t + λ'
563.5	1.0	2	17741	s + 1517	s + ξ
555.3	0.5	4	18003	u + 887	u + Ξ

Table II Continued

λ(nm)	Estimated Uncertainty (± nm)	Relative Intensity	Vacuum Corrected Energy (cm^{-1})	Assignment to Origins + Δν (cm^{-1})	Vibrational Identification
				t + 1402	t + λ' + θ
552.4	1.0	4	18098	t + 1497	t + ξ
543.2	0.4	9	18404	origin v	
540.1	0.3	10	18510	v + 106	v + β
530.1	0.6	7	18859	origin w	
521.8	0.7	9	19159	origin x	
519.5	0.4	12	19244	origin y	
517.6	1.0	9	19315	x + 156	x + δ
~510.0	2.0	8	19602	x + 443	x + η
503.5	0.2	30	19855	origin z	
501.2	1.5	15	19947	y + 92	y + β
495.5	0.2	32	20176	origin aa	
491.4	0.3	22	20344	origin bb	
484.5	0.3	18	20634	origin cc	
481.2	1.2	15	20776	origin dd	
474.7	1.2	60	21060	origin ee	
472.1	0.4	76	21176	ee + 116	ee + β
461.3	0.8	14	21672	aa + 1496	aa + ξ
455.4	0.5	12	21953	origin ff	
				ee + 893	ee + λ
450.0	0.3	14	22216	origin gg	
448.3	1.5	11	22300	cc + 1524	cc + ξ'
439.1	0.2	24	22767	origin hh	
429.3	0.2	15	23287	origin ii	
427.1	1.5	9	23407	origin jj	
				ii + 120	ii + β

Table II Continued

λ(nm)	Estimated Uncertainty (± nm)	Relative Intensity	Vacuum Corrected Energy (cm^{-1})	Assignment to Origins + Δν (cm^{-1})	Vibrational Identification
421.8	0.5	7	23701	ii + 414	ii + ζ
				hh + 934	hh + λ'
414.1	1.5	5	24142	ii + 855	ii + Ξ
411.3	0.5	7	24306	origin kk	
403.9	0.7	8	24752	origin ℓℓ	
402.5	1.0	8	24838	ii + 1551	ii + ξ"
397.9	0.2	13	25125	origin mm	
396.5	1.5	10	25214	mm + 89	mm + β
393.5	1.0	13	25406	origin nn	
390.2	0.2	23	25621	mm + 496	mm + θ
				ℓℓ + 869	ℓℓ + Ξ
385.9	0.2	25	25906	origin oo	
~380.0	7.5	~ 10	26308	oo + 402	oo + ζ
369.2	2.0	~ 4	27078	origin pp	
367.1	1.5	~ 4	27233	origin qq	
360.0	0.2	9	27770	origin rr	
355.3	0.3	12	28137	origin ss	

Table III. Vibrational energies associated with $Np(BD_4)_4/Zr(Bd_4)_4$ origins

Origin	xx	β	δ	ε	ζ	η'	η	θ	χ	κ	Ξ	λ	λ'	ξ	ξ'	ξ''
a	43	121	156	172	409	430	452	474	793	803	866	914	929	1516	1531	1542
b	38	119	168	185	415	–	459	–	805	827	846	–	923	1518	–	1548
c	–	96	160	–	412	–	457	–	–	–	–	893	929	–	–	–
d	52	122	168	–	–	425	455	–	799	–	866	920	–	1515	–	–
e	48	123	165	–	413	–	456	–	764	–	–	914	–	–	–	–
f	–	–	–	172	413	–	–	465	–	826	–	–	–	–	–	–
g	–	–	148	–	–	–	443	–	–	–	853	–	–	–	–	–
h	–	109	–	–	–	–	453	–	793	835	–	914	–	–	–	–
i	–	–	146	194	–	–	461	–	761	–	–	–	–	–	–	–
j	42	121	–	–	–	–	453	–	–	–	–	–	–	–	–	–
k	–	114	–	–	–	–	–	–	–	–	–	–	–	–	–	–
ℓ	–	130	–	–	–	–	–	–	–	806	–	–	–	1493	–	–
m	–	–	152	–	–	–	456	–	–	–	–	–	–	–	–	–
n	–	–	–	–	–	–	–	–	–	–	–	–	–	–	–	–
o	–	–	145	–	–	–	456	–	–	831	–	–	930	–	–	–
p	–	117	–	–	–	–	–	479	771	–	–	–	930	1512	–	–
q	–	99	168	–	–	–	451	–	–	–	–	–	954	–	–	–
r	–	–	–	–	414	–	–	–	–	–	–	–	–	–	–	–
s	–	–	–	–	–	–	–	–	–	–	–	–	924	1517	–	–
t	–	–	–	–	–	–	–	464	–	–	–	–	938	1497	–	–
u	–	–	–	–	–	423	–	–	–	–	887	–	–	–	–	–
v	–	106	–	–	–	–	–	–	–	–	–	–	–	–	–	–
w	–	–	–	–	–	–	–	–	–	–	–	–	–	–	–	–
x	–	–	156	–	–	–	443	–	–	–	–	–	–	–	–	–
y	–	92	–	–	–	–	–	–	–	–	–	–	–	–	–	–
z	–	–	–	–	–	–	–	–	–	–	–	–	–	–	–	–
aa	–	–	–	–	–	–	–	–	–	–	–	–	–	1496	–	–
bb	–	–	–	–	–	–	–	–	–	–	–	–	–	–	–	–
cc	–	–	–	–	–	–	–	–	–	–	–	–	–	–	1524	–
dd	–	–	–	–	–	–	–	–	–	–	–	–	–	–	–	–

Table III. Continued

Origin	xx	β	δ	ε	ζ	η'	η	θ	χ	κ	Ξ	λ	λ'	ξ	ξ'	ξ''
ee	–	116	–	–	–	–	–	–	–	–	–	893	–	–	–	–
ff	–	–	–	–	–	–	–	–	–	–	–	–	–	–	–	–
gg	–	–	–	–	–	–	–	–	–	–	–	–	–	–	–	–
hh	–	–	–	–	–	–	–	–	–	–	–	–	934	–	–	–
ii	–	120	–	–	414	–	–	–	–	–	855	–	–	–	–	1551
jj	–	–	–	–	–	–	–	–	–	–	–	–	–	–	–	–
kk	–	–	–	–	–	–	–	–	–	–	–	–	–	–	–	–
ℓℓ	–	–	–	–	–	–	–	–	–	–	869	–	–	–	–	–
mm	–	89	–	–	–	–	–	496	–	–	–	–	–	–	–	–
nn	–	–	–	–	–	–	–	–	–	–	–	–	–	–	–	–
oo	–	–	–	–	402	–	–	–	–	–	–	–	–	–	–	–
pp	–	–	–	–	–	–	–	–	–	–	–	–	–	–	–	–
qq	–	–	–	–	–	–	–	–	–	–	–	–	–	–	–	–
rr	–	–	–	–	–	–	–	–	–	–	–	–	–	–	–	–

Table IV. HFR parameters (cm^{-1}) for U^{4+} and Np^{4+}

	U^{4+}	Np^{4+}
F^2	76652	79831
F^4	50147	52279
F^6	36828	38413
ζ	2092	2377
M^0	0.773	0.876
M^2	0.430	0.487
M^4	0.299	0.339

Table V. Parameter values (cm^{-1}) for trivalent and tetravalent Np and U[a]

	$Np(BD_4)_4$/ $Zr(BD_4)_4$	$U(BD_4)_4$/ $Hf(BD_4)_4$[b]	$U^{3+}:LaCl_3$[c]	$Np^{3+}:LaCl_3$[c]
F^2	46689(415)	41280(175)	39715(218)	44907(161)
F^4	43239(645)	40013(826)	33537(302)	36918(245)
F^6	26303(722)	22554(625)	23670(211)	25766(221)
ζ	2089(10)	1782(12)	1623(4)	1938(2)
α	40(2)	38(2)	27.6(0.9)	31.5(0.3)
β	[-600]	[-648]	-722(33)	-740(18)
γ	[1200]	[1200]	[1000]	899(70)
M^0	[0.88]	[0.987]	[0.67]	0.68(0.17)
M^2	[0.49]	[0.550]	d	d
M^4	[0.34]	[0.384]	d	d
P^2	[500]	[500]	1276(104)[e]	894(14)[e]
P^4	[500]	[500]	-	-
P^6	[500]	[500]	-	-
T^2	[278]	-	217(90)	278(22)
T^3	[44]	-	63(13)	44(7)
T^4	[64]	-	255(23)	64(7)
T^6	[-361]	-	-107(49)	-361(18)
T^7	[434]	-	617(78)	434(22)
T^8	[353]	-	[350]	353(17)
B_0^4	-2722(182)	-2445(124)	-532(139)	-632(48)
B_0^6	-5070(69)	-5371(81)	-1438(113)	-1625(52)

Table V continued.

	$Np(BD_4)_4$/ $Zr(BD_4)_4$	$U(BD_4)_4$/ $Hf(BD_4)_4$[b]	$U^{3+}:LaCl_3$[c]	$Np^{3+}:LaCl_3$[c]
σ	84	53	26	20
k	0.93[f]	0.91	-	-
ϕ_2	0.86[f]	0.81	-	-
r_{42}	0.93	0.97	0.84	0.82

[a] rms errors are in ( ). Values in [ ] were held fixed.
[b] Ref. 2.
[c] Ref. 14.
[d] M^2 and M^4 constrained to vary as $M^2/M^0 = 0.56$, $M^4/M^0 = 0.38$.
[e] P^4 and P^6 constrained to vary as $P^4/P^2 = 0.75$, $P^6/P^2 = 0.50$.
[f] Based on estimated free-ion parameters $\zeta = 2253$ and $F^2 = 54463$ cm^{-1}.

Table VI. Observed and calculated energy levels (cm^{-1}) of $Np(BD_4)_4/Zr(BD_4)_4$

Γ	E_{calc}	E_{obs}	ΔE[a]	Eigenvector[b]
6	0	0	0	$82\ ^4I_{9/2} + 10\ ^2H2_{9/2}$
8	457	–	–	$75\ ^4I_{9/2} + 10\ ^2H2_{9/2}$
8	2205	–	–	$68\ ^4I_{9/2} + 17\ ^2H2_{9/2}$
8	5620	5605	15	$67\ ^4I_{11/2} + 10\ ^4F_{3/2}$
6	7193	–	–	$86\ ^4I_{I_{11/2}} + 3\ ^2H2_{11/2}$
8	7193	7083	110	$66\ ^4I_{11/2} + 9\ ^4I_{9/2}$
7	7490	7594	104	$85\ ^4I_{11/2} + 6\ ^4I_{13/2}$
8	9387	9281	106	$39\ ^4F_3 + 16\ ^2D1_{3/2}$
7	9596	9571	25	$49\ ^4I_{13/2} + 16\ ^4F_{5/2}$
8	10777	10709	68	$45\ ^4I_{13/2} + 9\ ^4I_{15/2}$
6	11575	–	–	$81\ ^4I_{13/2} + 5\ ^4I_{15/2}$
8	11579	11535	44	$38\ ^4I_{13/2} + 14\ ^4F_{5/2}$
7	12277	12170	108	$64\ ^4I_{13/2} + 9\ ^4F_{7/2}$
8	12598	12623	–25	$18\ ^2H2_{9/2} + 16\ ^4I_{9/2}$
8	13003	12963	40	$21\ ^2H2_{9/2} + 11\ ^2G1_{9/2}$
8	13327	13416	–89	$19\ ^4I_{13/2} + 15\ ^4F_{5/2}$
6	13614	–	–	$30\ ^2H2_{9/2} + 11\ ^4F_{7/2}$
8	13741	13778	–37	$29\ ^4G_{5/2} + 26\ ^4I_{15/2}$
7	13929	14006	–77	$43\ ^4I_{15/2} + 30\ ^4I_{13/2}$
7	14297	14370	–73	$27\ ^4I_{13/2} + 25\ ^4G_{5/2}$
8	14375	14439	–64	$18\ ^4I_{15/2} + 17\ ^4G_{5/2}$

Table VI continued.

Γ	E_{calc}	E_{obs}	ΔE^a	Eigenvector[b]
6	14584	-	-	44 $^4F_{7/2}$ + 15 $^2G1_{7/2}$
7	14736	14791	-55	40 $^4F_{5/2}$ + 28 $^4G_{5/2}$
8	15279	15270	9	31 $^4F_{7/2}$ + 17 $^2G1_{7/2}$
7	15945	15889	-56	27 $^4F_{7/2}$ + 20 $^2G1_{7/2}$
8	16149	16224	-75	30 $^4I_{15/2}$ + 14 $^4S_{3/2}$
6	16549	-	-	42 $^4I_{15/2}$ + 15 $^2K_{15/2}$
8	16628	16601	27	33 $^4G_{7/2}$ + 24 $^4I_{15/2}$
8	17074	17116	-42	54 $^4I_{15/2}$ + 11 $^2K_{15/2}$
6	17682	-	-	41 $^4G_{7/2}$ + 17 $^4F_{7/2}$
7	18552	18404	148	51 $^4G_{7/2}$ + 22 $^4F_{7/2}$
8	18814	18859	-45	18 $^4G_{7/2}$ + 9 $^4F_{9/2}$
8	19048	19159	-111	21 $^2H2_{11/2}$ 8 $^4G_{7/2}$
6	19221	-	-	21 $^2P_{1/2}$ + 15 $^4D_{1/2}$
8	19234	19244	-10	16 $^2H2_{11/2}$ + 11 $^4G_{11/2}$
8	19706	19885	-	32 $^4K_{13/2}$ + 28 $^4F_{9/2}$
6	19725	-	-	21 $^4G_{7/2}$ + 20 $^4F_{9/2}$
7	20190	20176	14	49 $^2K_{13/2}$ + 9 $^4I_{13/2}$
8	20324	20344	-20	26 $^4F_{9/2}$ + 11 $^4I_{15/2}$
8	20668	20634	34	12 $^2H2_{11/2}$ + 11 $^4G_{9/2}$
7	20684	20776	-92	29 $^2H2_{11/2}$ + 15 $^2K_{13/2}$
6	21008	-	-	27 $^2K_{13/2}$ + 16 $^2G_{9/2}$

Table VI continued.

Γ	E_{calc}	E_{obs}	ΔE[a]	Eigenvector[b]
8	21110	21060	50	46 $^4G_{9/2}$ + 10 $^4D_{5/2}$
8	21453	–	–	20 $^2H2_{11/2}$ + 15 $^2K_{13/2}$
6	21831	–	–	25 $^2G1_{7/2}$ + 19 $^2G2_{7/2}$
8	22092	21953	139	23 $^2K_{13/2}$ + 13 $^4F_{7/2}$
7	22220	22216	4	66 $^2K_{13/2}$ + 6 $^4D_{5/2}$
7	22526	–	–	24 $^2G1_{7/2}$ + 15 $^4F_{7/2}$
8	22561	–	–	29 $^4G_{9/2}$ + 12 $^2H2_{11/2}$
6	22576	–	–	27 $^4D_{1/2}$ + 17 $^2P_{1/2}$
7	22643	22767	–124	18 $^4D_{5/2}$ + 18 $^2H2_{11/2}$
8	22230	23287	–57	36 $^2K_{13/2}$ + 17 $^4G_{9/2}$
6	23419	–	–	24 $^4G_{9/2}$ + 17 $^2K_{13/2}$
8	23421	23407	14	12 $^2L_{15/2}$ + 10 $^4G_{9/2}$
8	24291	24306	–15	19 $^4D_{5/2}$ + 13 $^2K_{15/2}$
7	24443	–	–	38 $^2K_{15/2}$ + 24 $^2L_{15/2}$
6	24621	–	–	19 $^2K_{15/2}$ + 14 $^2L_{15/2}$
8	24641	24752	–111	27 $^4D_{3/2}$ + 7 $^4G_{9/2}$
8	25223	25125	98	15 $^2L_{15/2}$ + 11 $^2K_{15/2}$
8	25399	25406	–7	17 $^2H1_{11/2}$ + 19 $^2L_{15/2}$
8	25897	25906	–	19 $^4G_{11/2}$ + 18 $^2D1_{5/2}$
7	25976	–	–	32 $^2H1_{11/2}$ + 24 $^2I_{11/2}$
8	26137	–	–	24 $^2H1_{11/2}$ + 19 $^4G_{11/2}$

Table VI continued.

Γ	E_{calc}	E_{obs}	ΔE^a	Eigenvector[b]
6	26277	-	-	$28\ ^2L_{15/2} + 13\ ^2H1_{11/2}$
8	26595	-	-	$19\ ^2D_{5/2} + 16\ ^2L_{15/2}$
8	26864	-	-	$12\ ^2P_{3/2} + 11\ ^2G1_{9/2}$
8	27167	27078	89	$24\ ^2I_{11/2} + 19\ ^2H1_{11/2}$
7	27243	27233	10	$53\ ^2D1_{5/2} + 16\ ^2H1_{11/2}$
6	27702	27698	-	$17\ ^2I_{11/2} + 16\ ^2G1_{9/2}$
8	27949	27770	179	$31\ ^4G_{11/2} + 15\ ^2I_{11/2}$
7	28120	28137	17	$34\ ^4G_{11/2} + 29\ ^2I_{15/2}$
8	28741	-	-	$14\ ^2D2_{3/2} + 9\ ^2I_{13/2}$
6	28835	-	-	$27\ ^2P_{1/2} + 17\ ^2H1_{11/2}$
6	29021	-	-	$24\ ^4D_{9/2} + 15\ ^2I_{11/2}$
8	29379	-	-	$70\ ^4D_{7/2} + 4\ ^2F1_{7/2}$
6	29699	-	-	$38\ ^4D_{7/2} + 20\ ^4G_{11/2}$
7	29715	-	-	$79\ ^4D_{7/2} + 5\ ^2F1_{7/2}$

[a] $\Delta E = E_{calc} - E_{obs}$

[b] percentage of SLJ state, 2 largest components

Table VII. Parameter values (cm^{-1}) associated with the orthogonalized operators of Judd and Crosswhite[a]

	$Np(BD_4)_4$/ $Zr(BD_4)_4$	$U(BD_4)_4$/ $Hf(BD_4)_4$[b]	$U^{3+}:LaCl_3$[c]	$Np^{3+}:LaCl_3$[c]
F^2	46068	40689	39268	44360
F^4	43182	39956	33450	36721
F^6	29044	25154	25507	27753
α'	32.0	30.4	22	25.2
β'	-60	-44	9.9	-2.7
γ'	120	114	76	73
ϕ_2	0.85[d]	0.79	-	-
r_{42}	0.94	0.98	0.85	0.83

[a] Ref. 20
[b] Ref. 2
[c] Ref. 14
[d] Based on a predicted free-ion $F^2 = 54473\ cm^{-1}$

Table VIII. Calculated values for g_{Γ_6}

k^a	g_{Γ_6}	g_{exp}
1.0	2.377	
0.885	1.896	1.896 $[Np(BD_4)_4]$
0.862	1.799	1.799 $[Np(BH_3CH_3)_4]$

[a] $g = \langle \psi \| k\vec{L} + g_s\vec{S} \| \psi \rangle$

Figure Captions

Figure 1. 2 K optical absorption spectra of $Np(BH_4)_4$ and $Np(BD_4)_4$ in the 2000-1500 nm region.

Figure 2. 2 K optical absorption spectra of $Np(BH_4)_4$ and $Np(BD_4)_4$ in the 1400-350 nm region.

Figure 3. EPR spectrum of $Np(BD_4)_4/Zr(BD_4)_4$ at 2 K:

(a) X-band spectrum at 9.39 GHz;

(b) K-band spectrum at 24.2 GHz.

Figure 4. Energy level diagram for a Kramer doublet with $S' = 1/2$, $I = 5/2$, $g = 1.894$, $A = 0.114\ cm^{-1}$. Allowed transitions are indicated with vertical arrows; -.-.-: X-band, ____: K-band, ——: Q-band. Q-band transitions are only indicated below 11 kGauss.

Figure 5. Inverse paramagnetic susceptibility of $Np(BH_3CH_3)_4$;

ΔΔΔ: experimental data obtained at 5 kGauss.

A: calculated considering only $^4I_{9/2}$, $B_0^4 = -1461\ cm^{-1}$, $B_0^6 = -3274\ cm^{-1}$, orbital reduction factor $k = 0.82$.

B: calculated from the parameters in Table V, first column, with no orbital reduction factor.

C: same as B, but with an orbital reduction factor $k = 0.862$.

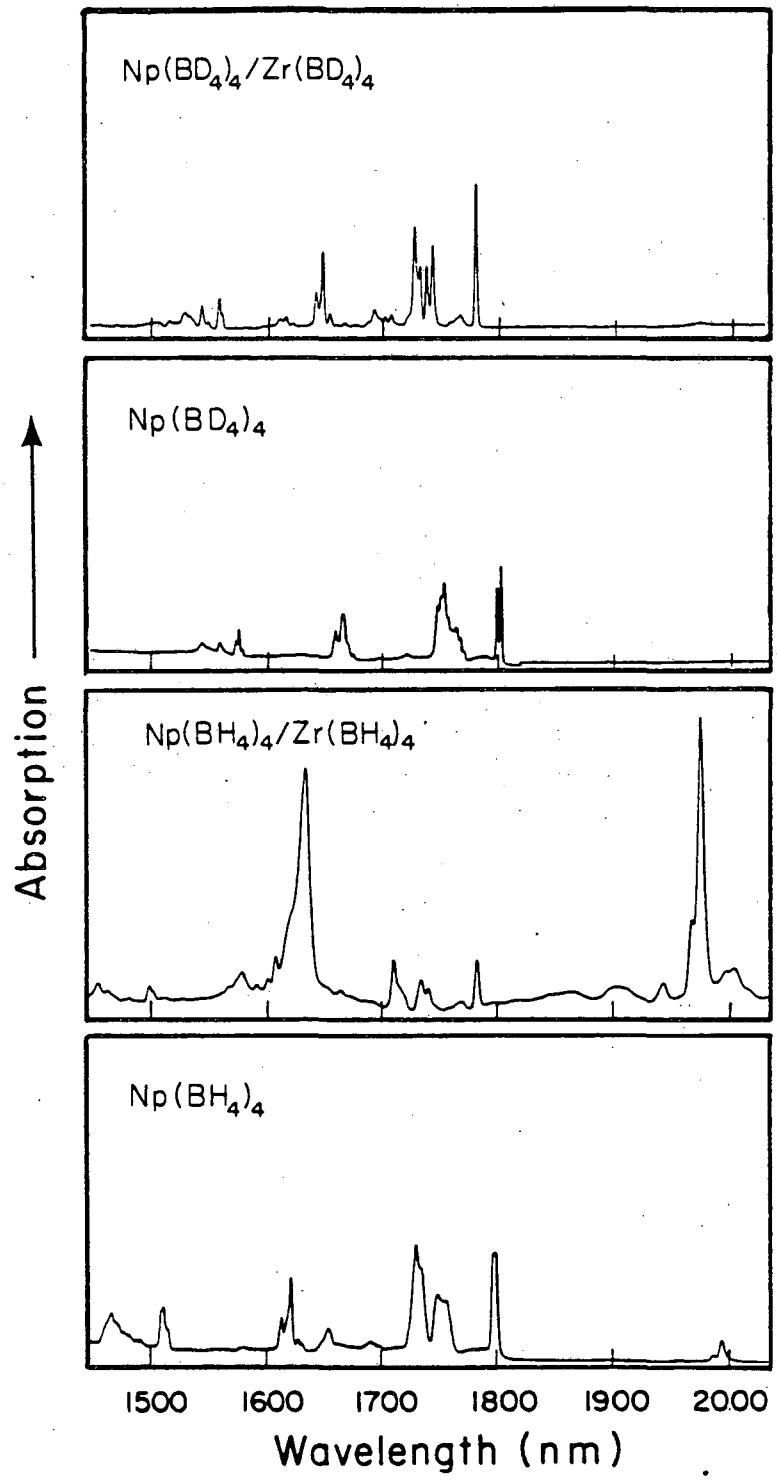

XBL7911-13259

Figure 1

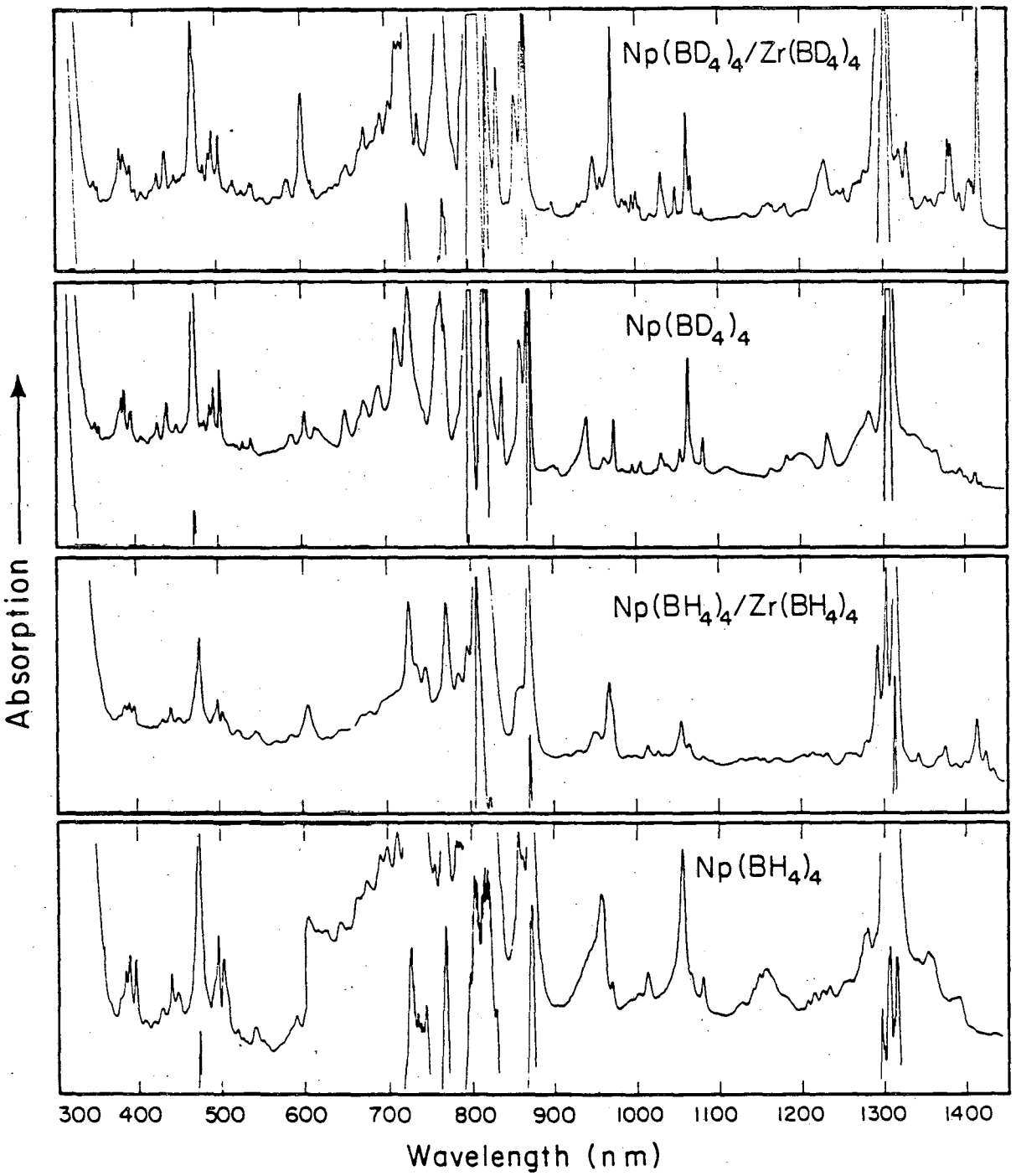
Np(BD4)4/Zr(BD4)4
Np(BD4)4
Np(BH4)4/Zr(BH4)4
Np(BH4)4
Absorption
300 400 500 600 700 800 900 1000 1100 1200 1300 1400
Wavelength (nm)
XBL 837-478

Figure 2

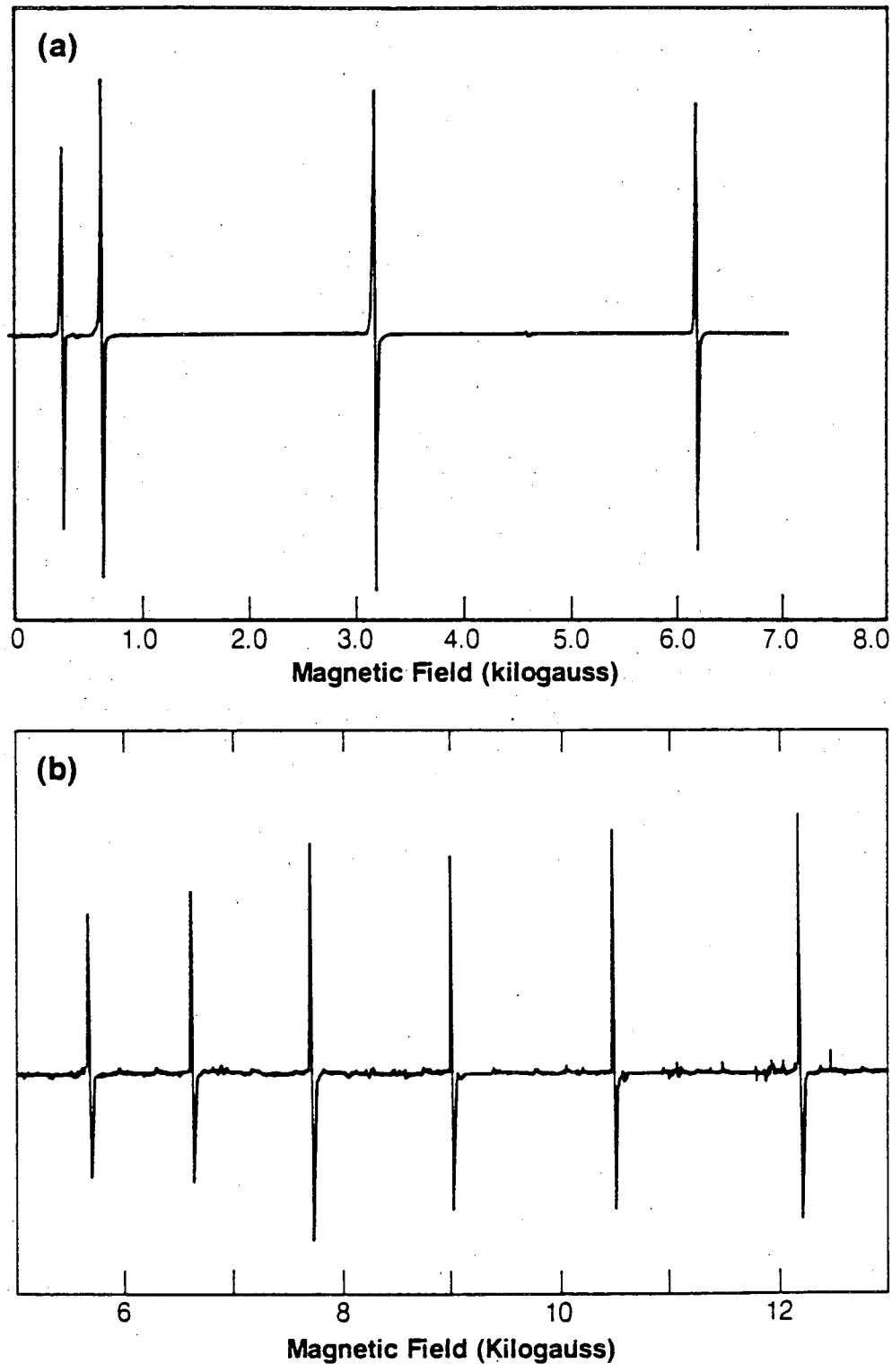

XBL 837-475

Figure 3

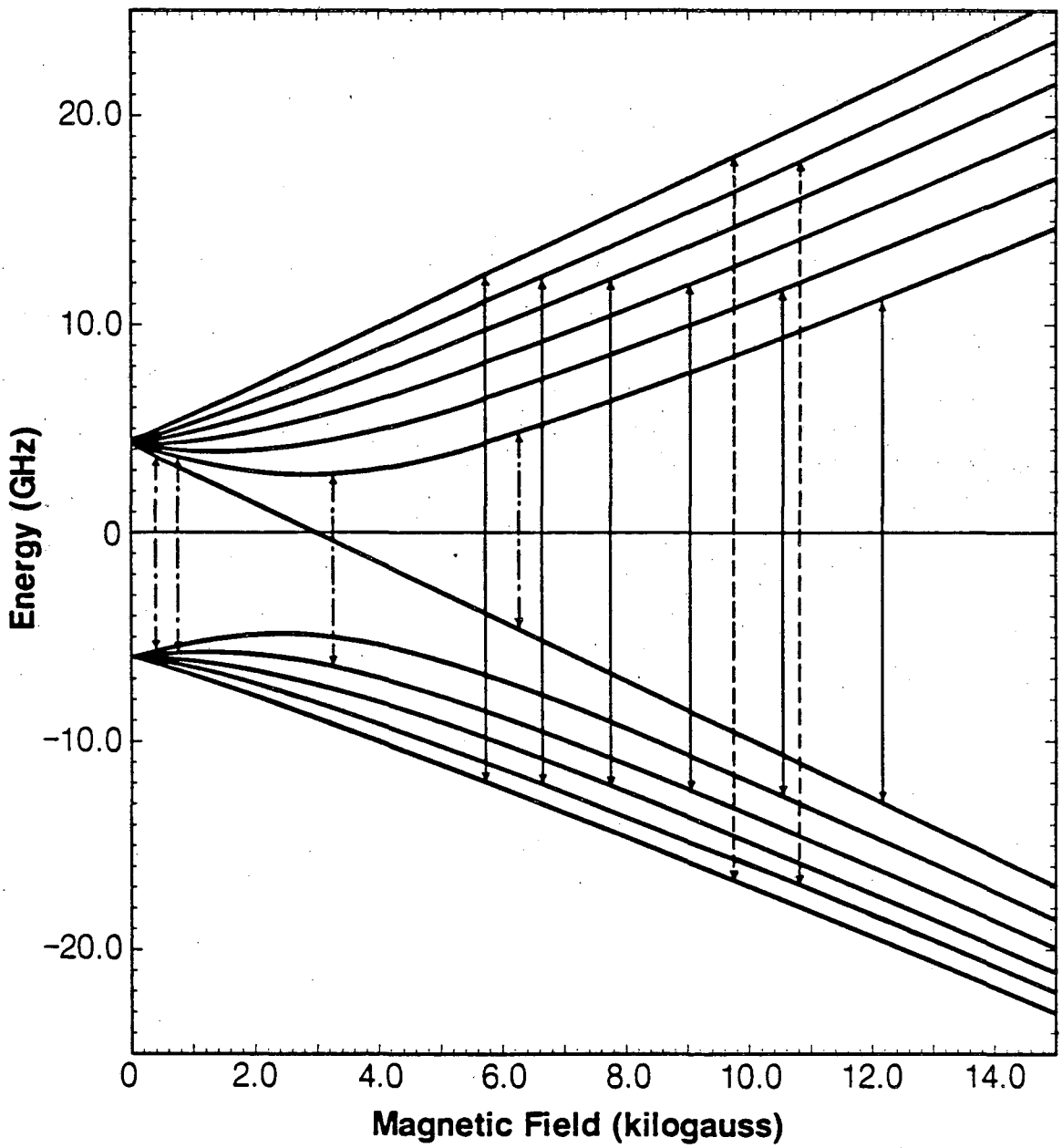

XBL 838-10938

Figure 4

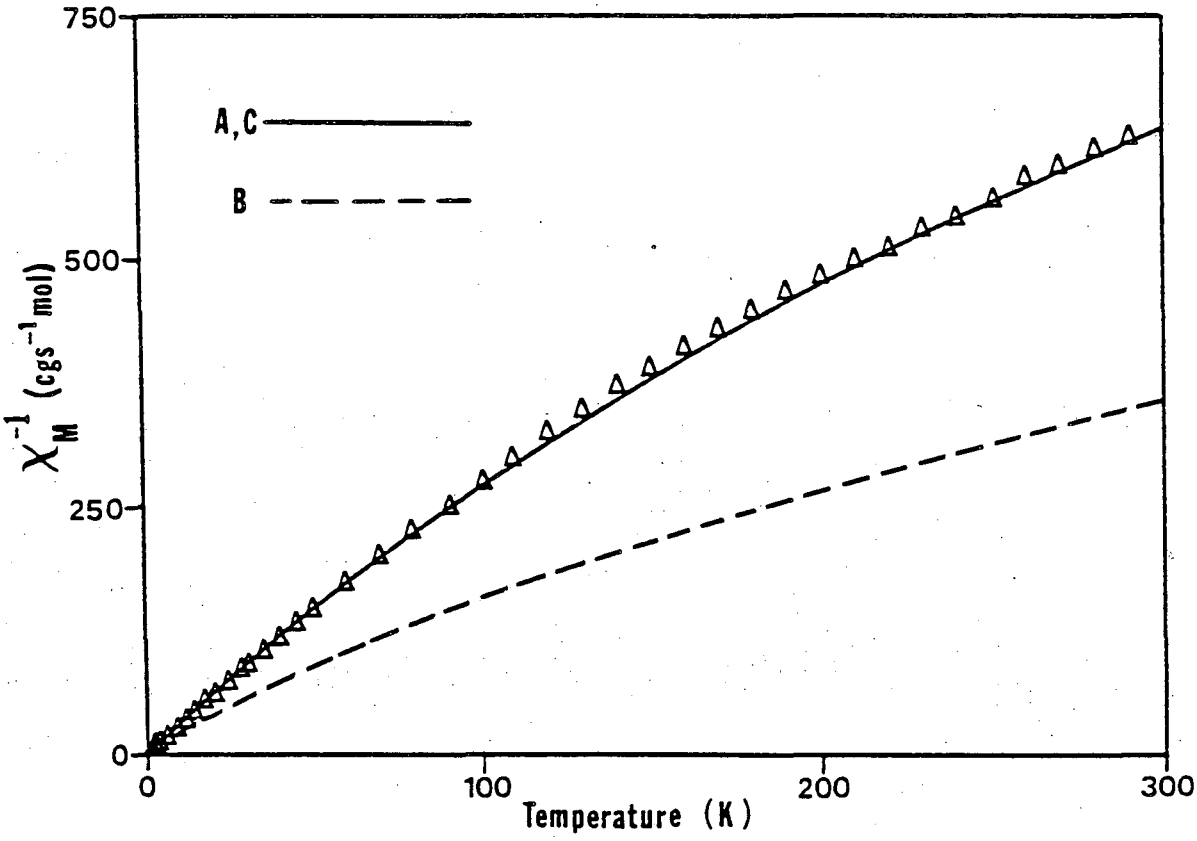

XBL 838-11024

Figure 5

This report was done with support from the Department of Energy. Any conclusions or opinions expressed in this report represent solely those of the author(s) and not necessarily those of The Regents of the University of California, the Lawrence Berkeley Laboratory or the Department of Energy.

Reference to a company or product name does not imply approval or recommendation of the product by the University of California or the U.S. Department of Energy to the exclusion of others that may be suitable.

TECHNICAL INFORMATION DEPARTMENT
LAWRENCE BERKELEY LABORATORY
UNIVERSITY OF CALIFORNIA
BERKELEY, CALIFORNIA 94720